



Regular Research Manuscript

Isolation and Performance Test of Green Low Dosage Hydrate Inhibitors from Local Materials for Improving Flow Assurance in Oil and Gas Industry

Julieth P. Kakwaya, Makungu M. Madirisha*, Kessy F. Kilulya, and Esther H. J. Lugwisha

Chemistry Department, University of Dar es Salaam, Dar es Salaam, Tanzania

†Corresponding author: makungumarco@udsm.ac.tz

ORCID: <https://orcid.org/0000-0002-4037-3974>

ABSTRACT

The formation of gas hydrates in oil and gas industry can be minimized or prevented by the use of inhibitors. This paper reports on hemicellulose and modified lignin as low dosage gas hydrate inhibitors (LDGHIs). LDGHIs were isolated from sugarcane bagasse (SCB), plant gum exudates (PGE) of Acacia trees, and coconut coir, and further characterized by Attenuated Total Reflectance - Fourier Transform Infrared (ATR-FTIR) spectrometer, porosimeter and thermogravimetric analyzer (TGA). The PGE and SCB yielded 77.75% and 12.38% of hemicellulose, respectively, while coconut coir yielded 35.59% of lignin which was modified to sodium lignosulfonate (SLS) to improve its solubility in water. The inhibition performance of the isolated hemicellulose and modified lignin on gas hydrate was evaluated in terms of percentages of water converted into gas hydrate. In the absence of inhibitors, a large percentage of water (75.20%) was converted to gas hydrates while in the presence of the hemicellulose, the minimum amount of water converted into gas hydrates was 43.37%. The inhibition ability of hemicellulose from PGE and SCB increased with an increase in concentration. The statistical test indicated no significant difference between the percentage of water that formed gas hydrates in the presence of hemicellulose from PGE and SCB ($n=4$, $p=0.06$ at $CI=95\%$). On the other hand, SLS promoted gas hydrates growth. In the presence of SLS, all liquid in the reactor was converted to gas hydrates. Thus, SLS may be used as a promoter for gas hydrates in natural gas storage and carbon dioxide sequestration while hemicellulose from both PGE and SCB as low dosage hydrate inhibitors.

ARTICLE INFO

First submitted: Oct. 14, 2022

Revised: Mar. 19, 2023

Accepted: Apr. 15, 2023

Published: June, 2023

Keywords: Gas hydrate, Low dosage gas hydrate inhibitor, Flow assurance, Oil and gas industry

INTRODUCTION

Gas hydrate (GH) formation is the major flow assurance problem that has raised concerns in oil and gas industry because of posing a significant hazard to conventional oil and gas drilling, and production operations (Folger, 2010; Arinkoola, 2009;

Paez et al., 2001a, 2001b). GHs tend to plug pipelines resulting in decreased production and/or complete shutdown, pipeline rupture, and posing risk to workers (Sami et al., 2013; Folger, 2010). Further, GHs lead to increased wellbore instability, wellbore-casing cementing failure, formation

damage, and drilling fluid gasification and foaming (Amodu, 2008). About 10 to 15% of production cost is spent on gas hydrate inhibition (Elgibaly and Elkamel, 2018; Makogon et al., 2004).

During gas hydrate formation (Figure 1), hydrogen bonding between water molecules leads to the formation of a metastable geometric structure (also known as lattice/crystal structure) with a cavity inside. The metastable geometric structure formed may have twelve, fourteen, or sixteen sides (Paez et al., 2001a). Later, gas molecules such as methane, ethane, propane, isobutane, hydrogen sulfide, carbon dioxide, and nitrogen occupy the cavity thus solid nuclei begin to form and start to grow (Okereke et al., 2020). This is followed by agglomeration of the solid nuclei in which large particles are formed as a result of contact between solid nuclei. When solid particles reach a critical size of 8-30 nm, the rapid growth of the crystals occurs (Paez et al., 2001a).

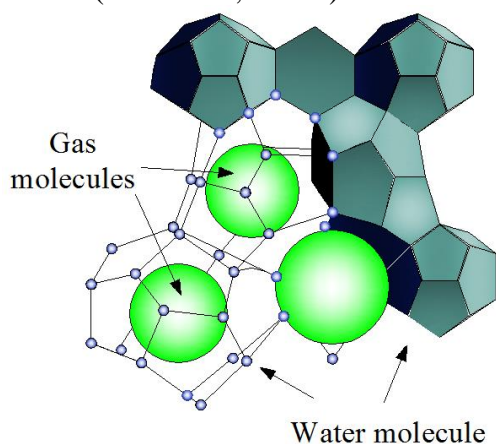


Figure. 1: Schematic diagram for the formation of gas hydrate (Source: Zarinabadi et al., 2011).

There are various methods for minimizing or preventing gas hydrate formation. These include removing water from the gas/oil stream, keeping an operating temperature above the hydrate equilibrium temperature, keeping an operating pressure below the hydrate equilibrium pressure, and/or injecting gas hydrate inhibitors (Igboanusi et al., 2011; Paez et al., 2001a, 2001b). These methods can be used separately or in

combination. Complete removal of water is difficult to achieve. Keeping an operating temperature above the hydrate equilibrium temperature is expensive (especially with long pipelines) as it is achieved by using line heaters or insulating pipelines. Depressurizing the system to keep the pressure below the hydrate equilibrium is impracticable since high pressure is required to transport fluid within pipelines (Igboanusi et al., 2011; Paez et al., 2001a). Thus, more efforts are nowadays directed toward the use of gas hydrate inhibitors which involve the injection of chemicals with inhibition ability (Kamal et al., 2016). Gas hydrate inhibitors that are currently in use are classified based on the mechanism of their action as thermodynamic hydrate inhibitors (THIs) and low dosage hydrate inhibitors (LDHIs). Thermodynamic hydrate inhibitors (THIs) are expensive, not environmentally friendly, and require a regeneration unit after use which increases operational costs. In addition, exposure to high heat on regeneration of THI like ethylene glycol has been reported to reduce its performance because it undergoes degradation and forms products such as glycolic, oxalic, and formic acids (Alharooni et al., 2015). Further, extreme conditions from deepwater oil/gas wells and large amounts (up to 50 wt %) for effective hydrate suppression have limited the application of THIs (Gupta and Sangwai, 2019; Igboanusi et al., 2011). Thus, efforts have recently been directed toward low dosage hydrate inhibitors (LDHIs) which are effective at lower concentrations up to 1 wt% (Farhadian et al., 2019; Perfeltd et al., 2014; Igboanusi et al., 2011).

Low dosage hydrate inhibitors (LDHIs) are classified as kinetic hydrate inhibitors and anti-agglomerants. Kinetic hydrate inhibitors (KHIs) are mostly water-soluble polymers that act by retarding nucleation and/or hydrate crystal growth thus, preventing the formation of hydrate plugs within pipeline during the residence time of hydrocarbons (Igboanusi et al., 2011). The

proposed mechanisms for the inhibition of KHIs include adsorption of the inhibitor on the hydrate crystal surface through its polar functional groups. This destructs the water hydrogen bond network hence creating a barrier for gas hydrate nucleation, and preventing guest molecules from occupying cavities through the interaction of functional groups of the inhibitor with open cavities of the hydrate surface (Kamal et al., 2016; Sa et al., 2013). Anti-agglomerants (AAs) are mostly surfactants that act by hindering the agglomeration of hydrate crystals into large sizes that can later lead to pipeline plugging (Wan et al., 2019; Kamal et al., 2016; Perrin et al., 2013). The formed solid nuclei are prevented from growing into hydrate plugs thus they are only transported as a slurry (Paez et al., 2001a). Application of green low dosage gas hydrate inhibitors from biomass such as amino acids (glycine and leucine), pyridinium-based ionic liquids, hydroxyethylcellulose, carboxymethylcellulose, chitosan, starch, pectin xanthan gum, guar gum, and gum arabic is reported as a promising alternative to THIs (Gupta and Sangwai, 2019; Sanatgar and Peyvandi, 2019; Ishmuratov et al., 2018; Jokandan et al., 2016; Xu et al., 2016; Sa et al., 2013). The application of green low dosage gas hydrate inhibitors from biomass to inhibit gas hydrates is still a premature research area that requires more exploration to find the most effective inhibitors. This paper therefore, reports on the isolation and

performance test of green low dosage gas hydrate inhibitors (kinetic gas hydrate inhibitors) from sugarcane bagasse and plant gum exudates of *Acacia* trees.

EXPERIMENTAL WORK

MATERIALS

Sugarcane bagasse (SCB), Figure 2a, was collected from the Students' Cafeteria of the University of Dar es Salaam while plant gum exudates (Figure 2b) were collected at Sejeli, Mtunduru, and Msweya villages of Mbande area in Dodoma region, Tanzania. Coconut husks (Figure 2c) were collected from Kidenge village in Kibaha district, Pwani. Sugarcane bagasse samples were dried under sunlight for three days, then cut into small pieces using a knife and ground using a laboratory mill at the Botany Department, University of Dar es Salaam. The plant gum exudates (PGE) samples were also ground using the same machine, all ground samples were sieved in a laboratory test sieve of 250 μm to obtain a fine powder. The prepared powder samples were then stored in labelled airtight plastic containers.

Analytical grade chemicals and reagents; sodium hydroxide, ethanol, and sodium chloride were purchased from Z. & K Company in Tanzania, whereas distilled water was obtained from the College of Engineering and Technology, University of Dar es Salaam.



Figure 2: Collected samples: (a) Plant gum exudates (b) Sugarcane bagasse (c) Coconut husks.

Extraction and Isolation of Hemicellulose and Lignin

Hemicellulose from plant gum powder was extracted according to Bilal et al. (2015). Sieved plant gum powder (100 g) was dispersed in 200 mL distilled water for 24 hours with irregular stirring. The solution was then filtered followed by addition of 350 mL ethanol to the filtrate that consequently resulted to formation of precipitates. The precipitates were then washed with ethanol four times and dried in an oven at 60 °C to constant weight. The dried precipitates were ground using a motor and pestle and then stored in airtight plastic bags for further analysis and use. The percentage yield of hemicellulose was calculated based on Equation (1).

$$\% \text{ Yield} = \frac{\text{Weight of dry isolate (g)}}{\text{Initial weight of raw material (g)}} \times 100$$

(1)

Hemicellulose from sugarcane bagasse (SCB) was extracted according to Plengnok and Jarukumjorn (2020) with some modifications. The sugarcane bagasse (SCB) powder was de-waxed with ethanol in the Soxhlet apparatus for 6 hours. The dewaxed sample was then dried in an oven at 60 °C to constant weight. 10 g of the dry dewaxed SCB sample were dissolved in 250 mL 0.5 M NaOH, the solution was then kept for 2 hours with magnetic stirring. The solution was filtered and the supernatant solution was kept while the residues were discarded. 6 M HCl was used to drop the pH of the supernatant solution from 13 to 5.50. The solution was then kept in a fridge for 24 hours. Thereafter, 350 mL ethanol was added to the solution, and precipitates were formed. The solution containing precipitates was centrifuged at 3500 RPM for 15 minutes. Precipitates settled at the bottom of the vials and were then removed and dried in an oven at 80 °C to constant weight. The dried precipitates were ground using a motor and pestle and then stored in airtight plastic bags for further analysis and use. The percentage yield of hemicellulose was calculated according to equation 1.

Lignin from coconut coir powder was extracted according to Panamgama and Peramune (2018) with some modifications. 10 g of coconut coir powder was dissolved in 200 mL 6 M NaOH. The solution was refluxed for 5 hours and then cooled. The cooled solution was filtered using Whatman filter paper (Cat No. 1001: 180) and the filtrate (also known as black liquor due to its black colour) was taken for further procedures while residues were discarded. 6 M H₂SO₄ was used to drop the pH of the black liquor from 12 to 1. The acidified solutions were then boiled at different time intervals (20, 30, 40, 50 and 60 minutes). Thereafter, the solutions were filtered with Whatman filter paper and the collected precipitates were washed with distilled water five times then dried in an oven at 105 °C to constant weight. The dried precipitates (lignin) were ground using motor and pestle and stored in airtight plastic bags for further analysis and use.

The modification of lignin to sodium lignosulfonate (SLS) was performed according to Nita et al. (2019). About 7 g of lignin powder was dissolved in 355 mL of 0.3 M NaHSO₃ and refluxed for 4 hours at 97 °C. The resulting solution was cooled and filtered. Thereafter, the filtrate was distilled at 100 °C to remove water. Then, 200 mL of ethanol was added to the cooled filtrate and stirred for 30 minutes. The resulting solution was then filtered and distilled at 79 °C to remove ethanol, and a light brown powder of SLS was collected and then dried in an oven at 80 °C to constant weight. The dried precipitates were ground using motor and pestle then stored in airtight plastic bags for further analysis and use.

Analytical Techniques

Functional groups of the isolated and modified samples were determined by ATR-FTIR spectrophotometer, Alpha Bruker. The IR spectra were recorded in the range of 400-4000 cm⁻¹ by taking 25 scans. During analysis, the crystal area was cleaned and background measurements

were done. For thermal stability of the samples, thermogravimetric analyzer (TGA) STA PT-1000 was used. Each sample was weighed in a sample pan and then heated from 30 – 600/700 °C at a heating rate of 5 °C min⁻¹.

For surface area of the samples, a nitrogen adsorption porosimeter (NOVA 1200e, PRUS Version 11.03, Quantachrome Corporation, Japan) was used. The device was warmed up for 30 minutes before the analysis. Later, a sample was filled in an instrument-specific glass holder and weighed on an analytical balance followed by degassed for 3 hours at a temperature of 160 °C with a reduced pressure. Degassing was done to remove impurities. The real porosimeter test was done by allowing boiling nitrogen gas at 77.35 K to be adsorbed by the degassed sample. The difference in volume adsorbed at different fractions of equilibrium and saturation pressures of nitrogen were recorded automatically and the characteristic isotherm was generated by NOVA Win software (PRUS Version 11.03). The isotherm was used to determine the BET (Brunauer-Emmett-Teller) surface area. The BET surface area (BET-SA) is the summation of both the external area and pore area.

Performance test

The performance test of the prepared gas hydrate inhibitors was done according to Farhadian et al. (2019) with some modifications. The performance test experiments were conducted on a Pressure Reactor available at the School of Mines and Geosciences (SoMG), University of Dar es Salaam. The main body of the Pressure Reactor is made of stainless steel with a total volume of 2000 mL and the design safe pressure and temperature are 2000 psi and 350 °C respectively. The pressure reactor is furnished with a

temperature controller (PARR 4843) which is designed to control temperature, pressure, and speed within the reactor. The controller consists of a type J (Iron-constantan) thermocouple for temperature measurements with accuracy +/- 2 °C and a pressure sensor. It also consists of a DC motor and a speed control knob for controlling the stirring rate within the reactor. The pressure reactor also consists of a furnace for heating purposes. A cooling system (a chiller) was incorporated to ensure that a temperature of 5 °C is reached. In addition, a system was coupled with a CO₂ gas cylinder as shown in the experimental setup (Figure 3).

A solution of 3.5 wt% NaCl was prepared and used throughout all experiments to represent produced brine from geological reservoirs. The concentration of KHI and SLS was each prepared as 0.1, 0.5, and 1 wt% for performance test (Table 1). The volume of reaction mixture in the reactor was maintained between 150-500 mL. and stirred while purging three times with 5 bar CO₂. The reactor was then cooled to 5 °C and stirring was stopped and the reactor was pressurized to 59 bars. Pressure changes were observed while stirring at a constant rate for 2 hours. Control experiment in absence of KHI was prepared. Thereafter, performance tests of the inhibitors were conducted whereby the solution of brine and the prepared inhibitor (at different concentrations) was put in the reactor and similar procedures were repeated. The effectiveness of the gas hydrate inhibitor used was determined by changes in the volume of brine as per Equation 2.

$$H_g = \frac{V_i - V_f}{V_i} \times 100 \quad (2)$$

where H_g is effective gas hydrants, V_i and V_f stands for initial and final volume of the gas respectively.

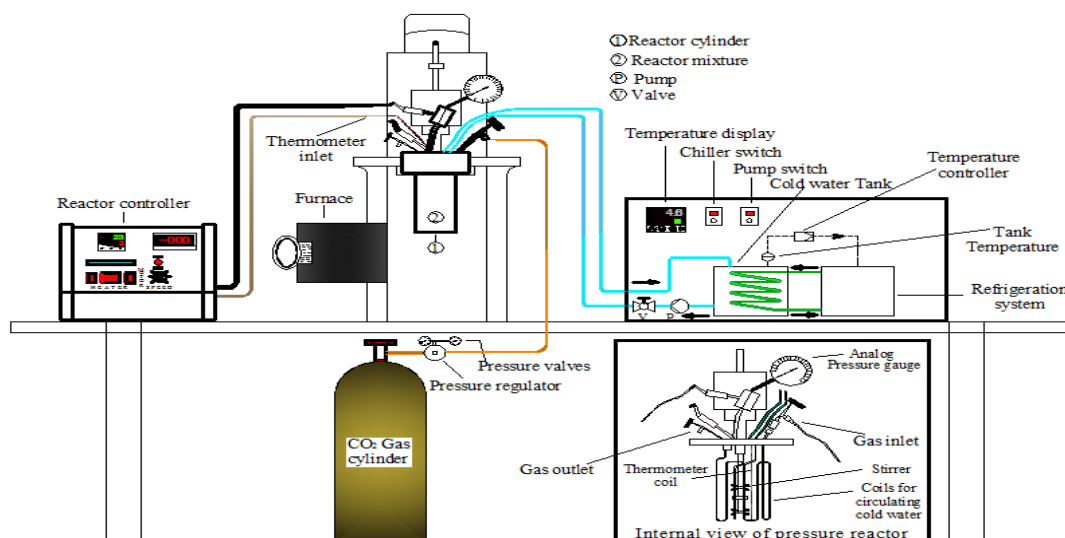


Figure 3: Experimental setup of performance test of gas hydrate inhibitors.

Table 1: Experimental Matrix for Performance Test of Hemicellulose and SLS

KHI	Concentration of inhibitor (wt%)	Initial volume (brine:n-hexane) (mL)
Control	0	500:0
Hemicellulose (PGE)	0.1	500:0
	0.5	500:0
	1.0	500:0
	1.0	500:0
Hemicellulose (SCB)	0.1	250:0
	0.5	250:0
	1.0	250:0
SLS	0.1	90:60
	0.5	90:60
	1.0	90:60

RESULTS AND DISCUSSION

Hemicellulose and Lignin Isolation

The plant gum exudate powder (100 g) and sugarcane bagasse powder (10 g) yielded 77.75% and 12.38% of hemicellulose, respectively. The extraction and isolation of hemicellulose from plant gum exudates were very effective due to the high solubility of the gums in water which in turn easily released the hemicellulose components. The recovered amount of hemicellulose from plant gum exudate was in agreement with what was reported by Mbuna and Mhinzi (2003). Moreover, the amount of hemicellulose isolated from sugarcane bagasse was in agreement with the amount reported by Sun et al. (2004) and Xie et al. (2020). The extraction of

hemicellulose from cell walls of lignocellulosic materials is limited by ester linkages between lignin and hemicellulose, and hydrogen bonding within individual polysaccharide components (Sun et al., 2004; Ebringerová and Heinze, 2000). For lignin isolation, it was observed that lignin yield increased as the boiling time of the acidified black liquor was increased. Also, the size of the precipitates increased with boiling time. The non-boiled acidified black liquor formed precipitates that were very small in size to the extent of clogging the filter paper. The non-boiled acidified solution difficultly passed through a filter paper unlike the boiled acidified black liquor whose precipitates were larger in size. The yield of lignin from acidified black liquor that was heated for 0, 20, 40

and 60 minutes was 9.98, 14.10, 14.56 and 35.59%, respectively. The modification of lignin to SLS yielded about 1.6 g (23% yield) of SLS from about 7 g of lignin. The possible reaction mechanism for conversion of lignin into SLS is shown in Figure 4.

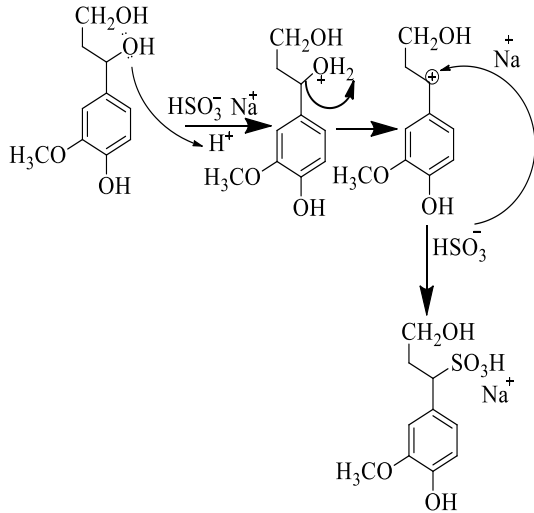


Figure 4: Mechanism of the sulfonation of lignin.

FTIR Characterization of Hemicellulose from Plant Gum Exudate

The FTIR spectrum of hemicellulose from plant gum exudate (Figure 5) shows functional groups such as an alkane, alkene, aldehyde, alcohol, and amine which are typical for complex polysaccharides such

as gum Arabic (Daoub et al., 2018; Bilal et al., 2015). A strong medium absorption band at 1602 cm^{-1} is observed which may be due to C=C stretch and amide NH bend. The two functional groups are reported to be from aliphatic and aromatic galactoproteins and amino acids (Daoub et al., 2018). A broad absorption band in the range of $3388\text{--}3229\text{ cm}^{-1}$ corresponds to the -OH functional group of aliphatic alcohols or phenols. A characteristic band for amines at $3100\text{--}3500\text{ cm}^{-1}$ might have been obscured by the broad band for the OH group (Daoub et al., 2018). At 2925 cm^{-1} a band is observed which may be due to the C-H stretches for alkanes and aldehydes. This also shows the presence of sugars, galactose, arabinose, and rhamnose. A small band at 1731 cm^{-1} is associated with a carbonyl stretch for saturated aldehydes (Daoub et al., 2018). C-O symmetric stretch and O-H bend are indicated by bands at 1411 and 1367 cm^{-1} , respectively. They are vibrations specific to glucuronic acids (Daoub et al., 2018). Bands at 1241 , 1144 , and 996 cm^{-1} are due to C-O stretches of either alcohol or ether. A sharp medium band for β -glycosidic linkage found in polysaccharides is observed at 836 cm^{-1} .

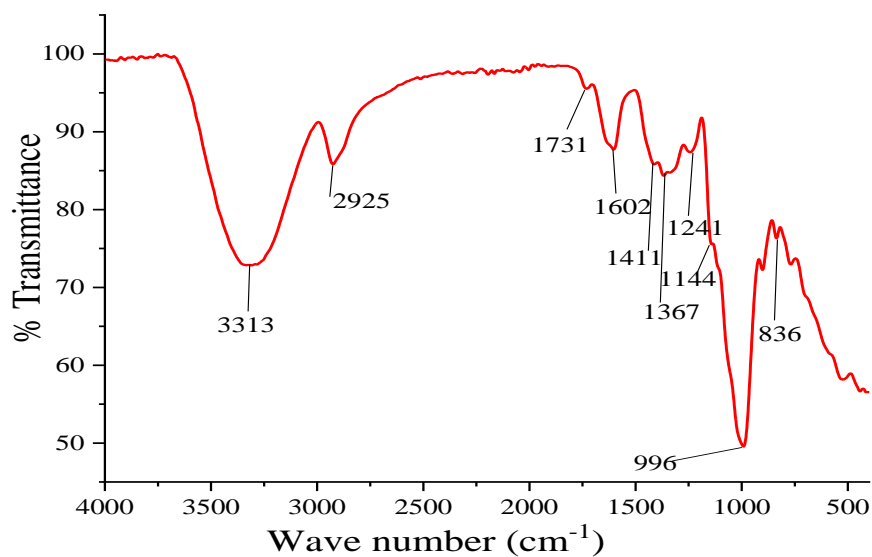


Figure 5: FTIR spectrum of hemicellulose from plant gum exudate.

FTIR Characterization of raw SCB, dewaxed SCB, and Hemicellulose from Dewaxed SCB

The FTIR spectra of the raw and dewaxed sample (Figure 6) show similar absorption peaks for -OH and C-H stretches. A decrease in the intensity of the peaks at 1733 cm^{-1} (for a carbonyl stretch), 1369 , and 1229 cm^{-1} (for C-H and C-O bend) is observed in the spectrum of the dewaxed SCB. Sugarcane wax is reported to contain long-chain aldehydes, long-chain primary alcohols, fatty acids, hydrocarbons, and esters (Qi et al., 2017), thus, a decrease in the intensities of the formerly mentioned peaks indicates that the dewaxing process was successfully done. A medium sharp peak that corresponds to β -glycosidic linkage (C-O-C) found in the polysaccharides is observed at 832 and 833 cm^{-1} in the spectra of raw and dewaxed SCB, respectively. The absence of a peak for a carbonyl stretch at 1733 cm^{-1} in the hemicellulose spectrum which was observed in the raw and dewaxed sample spectra indicates that alkaline treatment completely cleaved ester bonds from the hemicelluloses (Brienzo et al., 2009; Peng et al., 2009; Sun et al., 2004). A very small band at 1508 cm^{-1} indicates a very small amount of lignin remained in the hemicellulose fraction (Brienzo et al., 2009; Peng et al., 2009; Sun et al., 2004).

Besides, hemicellulose and lignin are linked together in such a way that their linkage is resistant to alkaline or peroxide treatment (Brienzo et al., 2016). However, the decrease in the intensity of this peak shows that fractions of lignin were separated from the hemicellulose fraction with only a very small amount of lignin left. For hemicellulose, a broad band absorption at 3289 cm^{-1} corresponds to -OH stretching vibrations while the absorption peak at 2922 cm^{-1} is due to C-H stretching vibrations. A carbonyl stretch due to absorbed water is observed at 1636 cm^{-1} (Peng et al., 2009; Sun et al., 2004). An intense peak at 1019 cm^{-1} is associated with C-O, C-C, C-OH, and C-O-C stretching and bending vibrations (Xie et al., 2020; Brienzo et al., 2009; Peng et al., 2009; Sun et al., 2004). Two low-intensity shoulders at 1152 and 896 cm^{-1} observed in the hemicellulose spectrum are reported to show the presence of arabinosyl side chains (Xie et al., 2020; Brienzo et al., 2009; Peng et al., 2009; Sun et al., 2004). C-H and C-O bends are associated with small bands at 1413 , 1371 , 1266 , and 1202 cm^{-1} . A very low-intensity band at 839 cm^{-1} is due to β -glycosidic linkage found in the hemicelluloses (Xie et al., 2020; Brienzo et al., 2009; Peng et al., 2009; Sun et al., 2004).

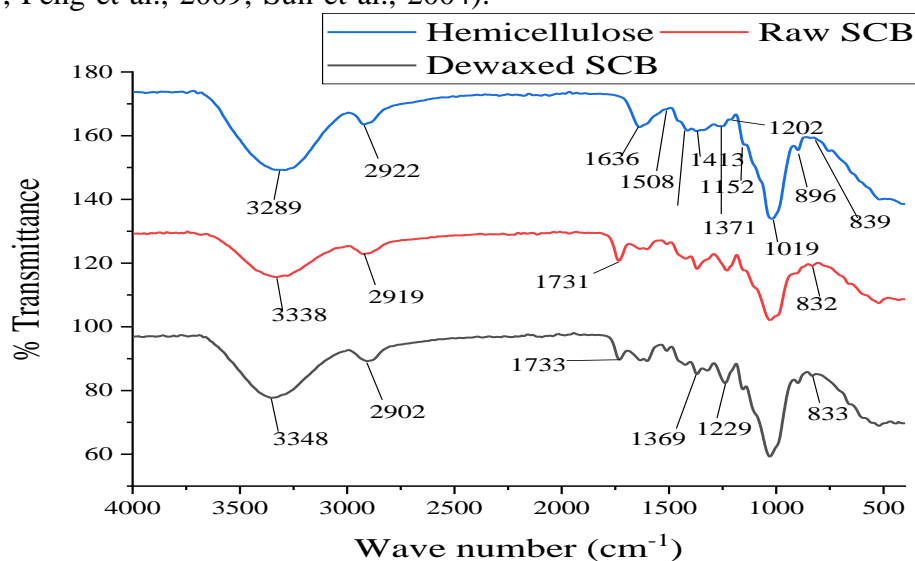


Figure 6: FTIR spectra of SCB, dewaxed SCB, and isolated hemicellulose.

FTIR Characterization of Lignin and Sodium Lignosulfonate

In the lignin spectra (Figure 7), C=C aromatic ring vibrations are shown by peaks appearing at 1601,1510 and 1419 cm^{-1} . They have been reported to be associated with phenyl-propane structures (Tejado et al. 2007, Panamgama and Peramune 2018). A broad band shown in the range 3460-3228 cm^{-1} is due to -OH stretching vibrations which are either phenolic and/or alcoholic (Boeriu et al. 2004, Tejado et al. 2007). A peak at 2936 cm^{-1} is due to C-H stretching vibrations of either CH_2 or CH_3 . The presence of unconjugated carbonyl is

shown by a stretching vibration at 1701 cm^{-1} . Peaks in the range 1300-1000 cm^{-1} may be due to C-O stretch from phenol or alkoxy groups. A peak at 894 cm^{-1} indicates the presence of β -glycosidic linkage in the polysaccharide. Nearly similar peaks are observed in the SLS spectrum with different peaks at 1101 and 1042 cm^{-1} for S=O symmetrical stretch and 616 cm^{-1} for SO_3 bend (Xu and Braterman 2003, Thungphotrakul et al. 2019, Daud et al. 2021). The presence of these peaks confirms that the sulfonation of lignin was successful.

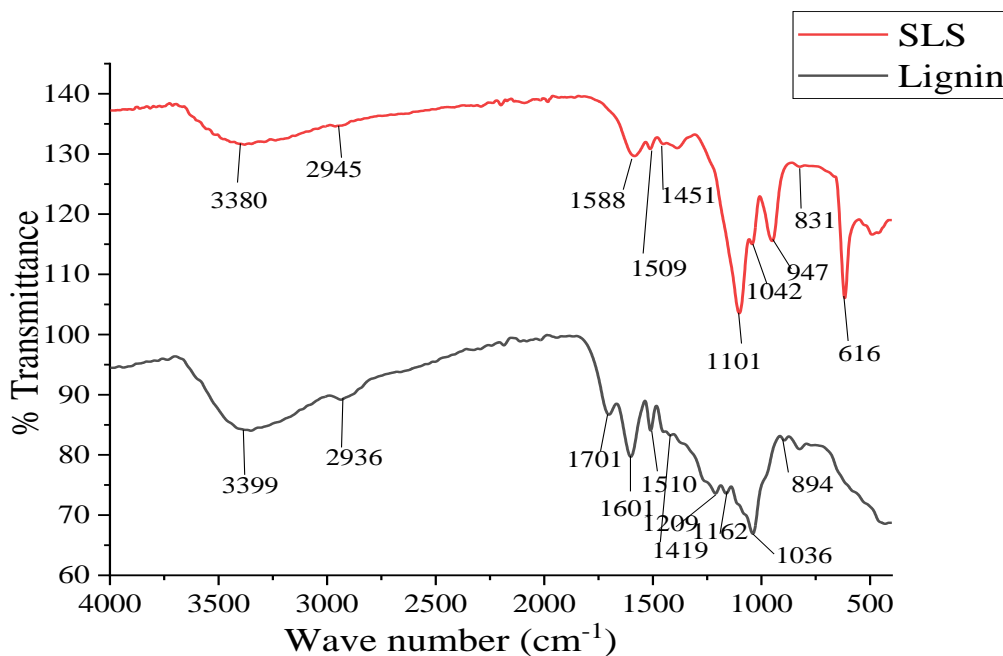


Figure 7: FTIR spectra of lignin and SLS.

Thermal Gravimetric Analysis (TGA) of hemicellulose from PGE and SCB

The thermogram (Figure 8a) for hemicellulose isolated from plant gum exudate obtained as the sample was heated from ambient temperature to 600 °C shows three mass loss events. The first event was observed between 30-100 °C accounting for 14% weight loss which is a result of loss of adsorbed and structural water bound to the polysaccharide (Daoub et al., 2018). The major weight loss event observed from 250-320 °C with about 51% weight loss was associated with hemicellulose

decomposition that is, depolymerization and cleavage of glycosyl units. This indicates that hemicellulose from plant gum exudate is thermally stable up to 250 °C. About 28% of the weight is lost from 400-520 °C, this may be due to the degradation of residues formed after hemicellulose degradation (Plengnok and Jarukumjorn, 2020). At temperatures above 486 °C, no significant weight changes were observed.

The thermogram (Figure 8b) for hemicellulose isolated from SCB obtained as the sample was heated from ambient

temperature to 600 °C shows three weight loss events. The loss of structural and absorbed water (about 13% weight loss) was observed between 30-100 °C. The presence of water in the sample is associated with the hydrophilic nature of the polysaccharide (Plengnok and Jarukumjorn, 2020). The major weight loss event was observed from 200-327 °C with about 57% weight loss. This may be due to the decomposition of side chains and saccharides units of the polysaccharide (Plengnok and Jarukumjorn, 2020; Sun et al., 2004). Thus, hemicellulose from SCB is thermally stable up to 200 °C. About 28% of the weight was lost between 400-520 °C. This may be due to the decomposition of substances formed during hemicellulose degradation and a small amount of bound lignin that remained in the hemicellulose fraction as discussed in the FTIR spectrum results (Plengnok and Jarukumjorn, 2020). Similar results were also reported by Peng et al. (2009), small deviations may be due to different extraction solvents used. At temperatures above 520 °C no any significant weight changes were observed. The thermogram (Figure 8c) for lignin isolated from coconut coir obtained as the sample was heated from ambient temperature to 700 °C shows three weight loss events. Loss of adsorbed water and high volatile compounds (accounting for about 16% weight loss) occurred from 40 - 100 °C (Panamgama and Peramune 2018). The second weight loss event occurred from 200 - 268 °C (accounting for about 19% weight loss) was due to the decomposition of propanoid side chains and aryl-alkyl-ether bonds of lignin. Thus, above 200 °C lignin starts to decompose (Vázquez-Torres et al. 1992, Brebu and Vasile 2010, Panamgama and Peramune 2018). The third weight loss event occurred between 268-446 °C (accounting for about 80% weight loss) with the highest weight loss rate occurring at 417 °C. This may be associated with demethylation and decomposition of phenol monomers of the

polysaccharide (Tejado et al. 2007, Brebu and Vasile 2010). Above 450 °C insignificant changes were observed which may be due to secondary reactions involving decomposition of condensable gases, lignin intermediates and char (Brebu and Vasile 2010).

The thermogram (Figure 8d) for modified lignin (SLS) obtained as the sample was heated from ambient temperature to 700 °C shows two weight loss events. Generally, about 20% of the initial weight is lost as the sample of SLS was heated. The small amount of weight loss for SLS shows that SLS is more thermally stable compared to lignin. This may be due to the decomposition mechanism of SLS since side chains mostly decomposes unlike lignin which involve decomposition of the main chain of the polymer. The presence of organically bound cations, that is Na⁺ in SLS accounts for dehydration and decarboxylation reactions that mainly occur as SLS decomposes (Lemes et al. 2010). During decomposition, sodium reacts with SO₂ and organic carbon forming Na₂SO₃/Na₂SO₄ and NaCO₃, respectively which can later decompose. This results in mercaptan, CO and CO₂ release (Lemes et al. 2010). Thus, two weight loss events are observed in the SLS thermogram. Loss of adsorbed water is observed between 40-107 °C with about 7% weight loss. About 11% weight is lost between 217-500 °C, this may be due to loss of mercaptans, SO₂, CO and CO₂ (Lemes et al. 2010).

Porosimeter results

BET surface areas (BET-SA) of hemicellulose from PGE and SCB, and modified lignin from coconut coir were determined and the results are shown in Table 2. From Table 2, the BET -SA of hemicellulose from SCB is larger than the BET-SA of SLS. However, the BET -SA of hemicellulose from PGE is smaller compared to all BET-SA.

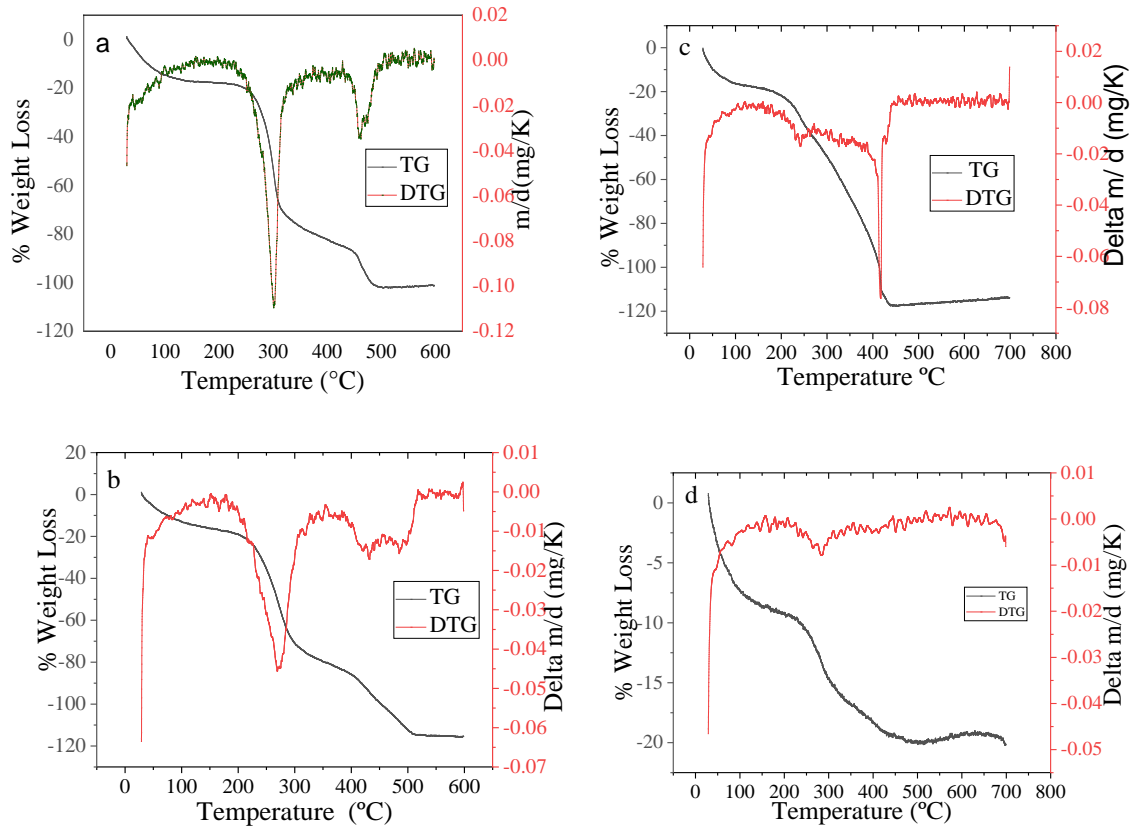


Figure 8: Thermograms for hemicellulose from (a) PGE, (b) SCB, (c) Lignin from coconut coir, and (d) SLS.

The higher the surface area of the hemicellulose or SLS, the higher the reactivity. To elaborate, the larger the surface area the hemicellulose or SLS cover, the more efficient its performance as a hydrate growth inhibitor will be. Therefore, hemicellulose from SCB would have more efficiency to inhibit gas hydrate followed by SLS and hemicellulose from PGE.

Table 2: BET surface area of the prepared inhibitors

Inhibitors	BET-SA (m ² /g)
Hemicellulose from PGE	2.224 × 10 ¹
Hemicellulose from SCB	2.766 × 10 ²
SLS	2.176 × 10 ²

Performance test results

During the performance test, pressure in control and inhibitor performance test experiments dropped immediately to about 50 bar in less than 1 minute just after the

reactor was pressurized to 59 bar (Figure 9). This implies that gas hydrates formed immediately just after conditions of appropriate temperature and pressure were reached in the presence of water and carbon dioxide gas. Since pressure dropped immediately and quickly even in the presence of inhibitors (hemicellulose from PGE and SCB, and SLS), the inhibitors used were not able to delay onset hydrate formation time. The continuation of pressure drop for about 6-10 minutes indicated that gas hydrates crystal growth was taking place. These observations were in agreement with Farhadian et al. (2019) who reported that, the formation of gas hydrates is indicated by a drop in pressure as a result of the trapping of gas molecules into water cavities. Further drops in pressure were an indication of growth of gas hydrates into large crystals.

Isolation and Performance Test of Green Low Dosage Hydrate Inhibitors from Local Materials for Improving Flow Assurance in Oil and Gas Industry

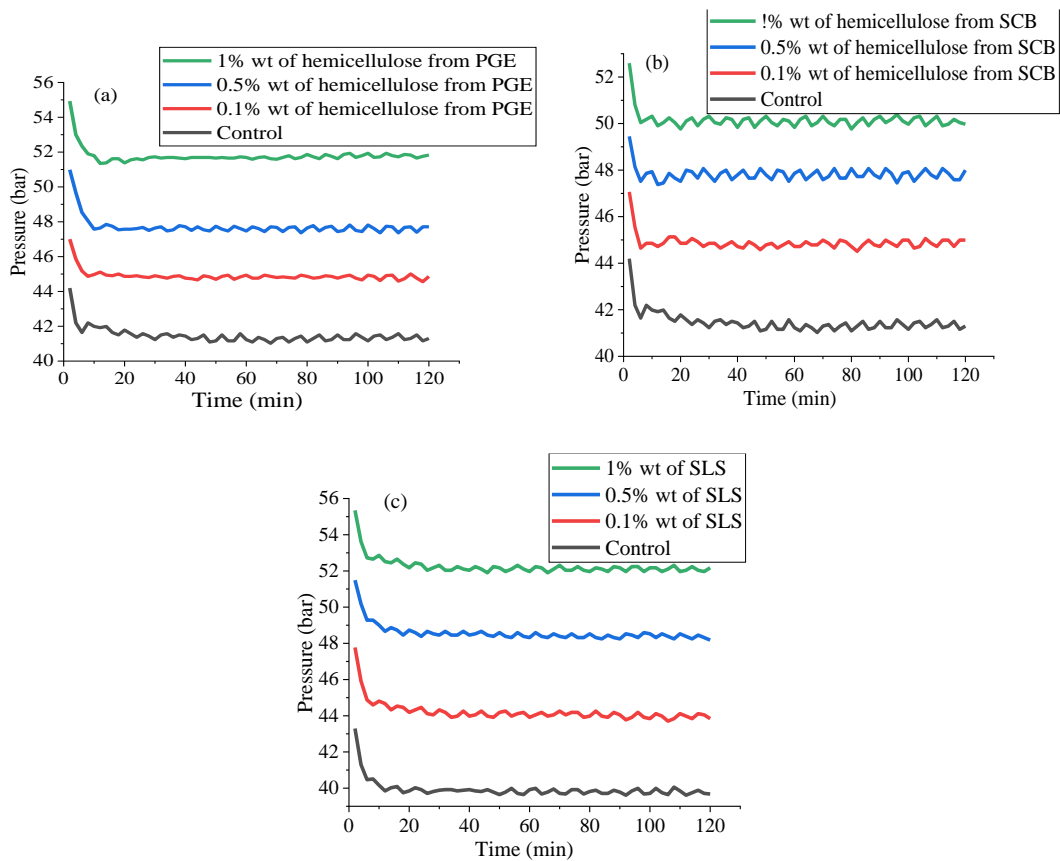


Figure 9: Variation of pressure with time during gas hydrate formation; (a) presence of hemicellulose from PGE (b) presence of hemicellulose from SCB (c) presence of SLS.

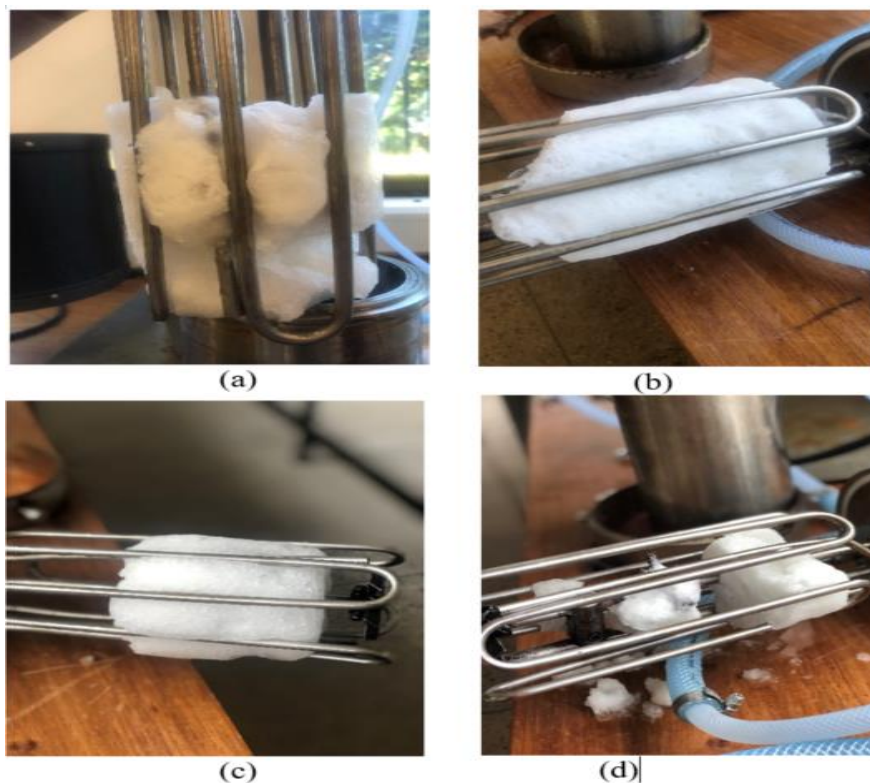


Figure 10: Gas hydrate crystals that formed: (a) absence of inhibitor (b) presence of 0.1 wt% inhibitor (c) presence of 0.5 wt% inhibitor (d) presence of 1.0 wt% inhibitor.

The effectiveness of the gas hydrate inhibitor used was determined based on percentages of water that formed gas hydrates. The percentages of water that

formed gas hydrates in the presence and absence of hemicellulose from PGE and SCB are shown in Table 3.

Table 3: Initial and final volume of brine in the reactor cylinder, and percentage of brine that formed gas hydrate during performance test of the inhibition ability of hemicellulose from PGE and SCB

Hemicellulose	Concentration of inhibitor (wt%)	Initial volume of brine (mL)	Final average volume of brine (mL)	Percentage of brine that formed gas hydrates (%)
Control	0	500	124.00	75.20
	0.1	500	187.15	62.57
PGE	0.5	500	247.25	50.55
	1.0	500	283.15	43.37
SCB	0.1	250	66.15	73.54
	0.5	250	71.55	71.38
	1.0	250	117.70	52.92

From Table 2, the smaller the percentage of water that formed gas hydrates in the presence of the inhibitor, the more effective the inhibitor. Further, the higher the percentage of water that formed gas hydrates in the presence of the inhibitor, the less effective the inhibitor. This observation was further supported by the size of the hydrate crystal as shown in Figure 10. Small amount of water is converted to gas hydrate in the presence of hemicellulose from PGE as compared to when hemicellulose from SCB. This observation can be explained in terms of number of hydroxyl groups as hemicellulose from PGE are rich in hydroxyl groups as compared to hemicellulose from SCB, and quickly dissolve in water. The inhibition ability of hemicellulose is accounted for by their high water solubility. When dissolved in water, fewer particles of hemicellulose were left undissolved thus reducing the ability of water to form cages through hydrogen bonding hence preventing the formation of gas hydrates.

Sodium lignosulfonate as a surfactant did not show any inhibition ability instead it promoted gas hydrate crystal growth. In the absence of SLS, with 150 mL as initial volume in the reactor (brine (90 ml) and *n*-hexane (60 mL)), the average amount of liquid that remained in the reactor was 58.5 mL (water (brine), 26.5 mL and *n*-hexane, 32 mL). Thus, 61% of liquid converted to gas hydrates. In the presence of 0.1, 0.5 and 1.0 wt% of SLS, no any liquid that remained in the reactor, all liquid was converted to gas hydrates. In addition, gas hydrate crystals that were formed were large in size compared to the one formed in the absence of the inhibitor as can be observed in Figure 11. Sodium lignosulfonate has a hydrophobic phenyl propane derivative with 3 - 6 carbons. It also contains carboxyl, sulfonic acid and phenolic hydroxyl groups as hydrophilic head groups. Its hydrophilic-lipophilic balance (HLB) has been reported to be 11.61 and has been classified as a surfactant that forms oil-in-water emulsion (Setiati et al. 2018).

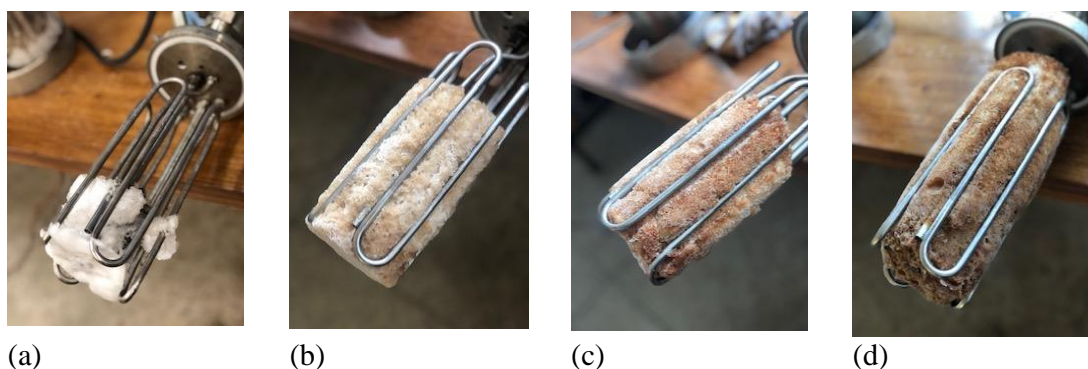


Figure 11: Gas hydrate crystals formed; (a) absence of SLS (b) 0.1wt% of SLS (c) 0.5 wt% of SLS (d) 1.0 wt% of SLS.

When oil is dispersed into the water phase, water becomes more accessible to be involved in gas hydrate formation process as a result gas hydrate crystal growth process is accelerated.

The inhibitors performance test results observed are not in agreement with the porosimeter results. This contradiction can be explained by the fact that the attractive force between the hydrate inhibitor and the hydrate surface is responsible for the adsorption to inhibit hydrate formation. To elaborate, spherical solutes with intermediate size are significantly stabilized at the hydrate surface whereas smaller and larger solutes exhibit lower adsorption affinity. This implies that hemicellulose from SCB, and SLS are smaller solutes (larger surface area) compared to hemicellulose from PGE which is likely to have an intermediate solute (smaller surface area).

Statistical T-tests

The p-value obtained from the paired t-test (0.06) shows that there is no statistically significant difference between the percentage of brine that formed gas hydrates in the presence of hemicellulose from PGE and SCB. The obtained value is greater than the accepted statistical value of 0.05 at a 95% confidence interval of the difference. Furthermore, the independent t-test results show that the p-value between the two groups (PGE and SCB hemicellulose) (0.185) on the continuous variable (percentage of brine converted into gas hydrate) is greater than the accepted statistical value of 0.05.

CONCLUSION

In this study, hemicellulose and lignin was isolated from plant gum exudates (PGE), sugarcane bagasse (SCB), and coconut coir. The isolated lignin was modified to sodium lignosulfonate (SLS) to improve its solubility in water. Plant gum exudates and sugarcane bagasse yielded 77.75% and 12.38% of hemicellulose, respectively. The extraction and isolation of hemicellulose from plant gum exudates was very effective due to the high solubility of the gums in water. In addition, gums contain large amount of hemicelluloses which accounts for the high yield of extraction and isolation. The relatively low yield of hemicellulose from SCB is due to strong ester linkages between lignin and hemicellulose and hydrogen bonding within individual polysaccharide components. These observations were in agreements with the literature (Ebringerová and Heinze 2000, Sun et al. 2004). On the other hand, the yield of lignin increased with an increase in boiling time of the acidified black liquor. The highest yield (35.59%) was obtained when the acidified black liquor was boiled for 60 minutes. Hemicellulose from PGE and SCB, lignin and sodium lignosulfonates (SLS) were confirmed by the results from FTIR and TGA.

During performance tests, hemicellulose from PGE and SCB showed the ability to prevent gas hydrate crystal growth as it was observed that less amount of water converted to gas hydrates in the presence of the inhibitors than in the absence of the inhibitors. Their inhibition ability increased

with an increase in concentration. In comparing the inhibition ability of hemicellulose isolated from PGE and SCB, hemicellulose from PGE was observed to be more effective since at 1% wt less amount of water (43.37%) was converted to gas hydrate than (52.92%) which was converted to gas hydrate when 1% wt of hemicellulose from SCB was present. The higher inhibition of hemicellulose from PGE is accounted by its more hydroxyl groups (as compared to hemicellulose from SCB) and ability to quickly dissolve in water. However, statistical test indicated no significant difference between the percentage of water that formed gas hydrates in the presence of hemicellulose from PGE and SCB ($n = 4, p = 0.06$ at $CI = 95\%$). Hence, the results affirm that hemicellulose from PGE and SCB can be an alternative low dosage hydrate inhibitor to prevent gas hydrate crystal growth in petroleum industry. In contrast, SLS promoted gas hydrate formation instead of slowing gas hydrate crystal growth process. SLS has been classified as a surfactant that forms oil in water emulsion unlike other surfactants that inhibit gas hydrates by forming water in oil emulsion.⁷³ Thus, SLS is not suitable to be applied in inhibiting gas hydrates instead it may be used as a promoter for gas hydrates formation to be used in natural gas storage and transportation, energy sources, cold energy, carbon dioxide capture and sequestration and gas separation (Sami et al. 2013, Zhang et al. 2020). Performance test results were not in agreement with the porosimeter results. Spherical intermediate sized solutes have been reported to have high adsorption affinity on the hydrate surface thereby impeding hydrate crystal growth than smaller and larger solutes. This accounts for the high inhibition ability of hemicellulose from PGE (intermediate solute with small surface area) than hemicellulose from SCB and SLS which are smaller solutes (large surface area).

ACKNOWLEDGMENTS

The authors are thankful to the University of Dar es Salaam for funding the project, the Chemistry Department for laboratory facilities and School of Mines and Geosciences laboratories of the University of Dar es Salaam for performance test experiments.

FUNDING

This study was fully sponsored by the University of Dar es Salaam through the merit scholarship program.

CONFLICT OF INTEREST

The authors declare no competing conflict of interest regarding the publication of this research work.

REFERENCES

- Alharooni K., Barifcani A., Pack D., Gubner R. and Ghodkay V. (2015). Inhibition Effects of Thermally Degraded MEG on Hydrate Formation for Gas Systems. *Journal of Petroleum Science and Engineering*, **135**: 608–617.
<https://doi.org/10.1016/j.petrol.2015.10.001>
- Amodu A. A. (2008). *Drilling Through Gas Hydrate Formations: Possible Problems and Suggested Solutions*. PhD thesis, Texas A&M University.
- Arinkoola A. O. (2009). Development of Empirical Correlations for Predicting Formation of Gas Hydrate. *International Journal of Oil, Gas and Coal Technology*, **2**(1): 24–43.
<https://doi.org/10.1504/IJOGCT.2009.023628>
- Bilal S., Mohammed-Dabo I., Dewu B., Momoh O. and Abubakar S. (2015). Refining and Characterisation of Gum Arabic Using Vacuum Filtration Method for Application in Oil and Gas Drilling Fluid Formulation. *Journal of Experimental Research*, **3**(2): 73–80.
www.er-journal.com%0Aer-journal.com/journals/Mohammed-Dabo_december_2015_3_2.pdf

- Brienzo M., Siqueira A. F. and Milagres A. M. (2009). Search for Optimum Conditions of Sugarcane Bagasse Hemicellulose Extraction. *Biochemical Engineering Journal*, **46**(2):199-204. <https://doi.org/10.1016/j.bej.2009.05.012>
- Brebu, M. and Vasile, C. (2010). Thermal degradation of lignin—a review. *Cellulose Chemistry & Technology*, **44**(9):353.
- Boeriu, C. G., Bravo, D., Gosselink, R. J. and van Dam, J. E. (2004). Characterisation of structure-dependent functional properties of lignin with infrared spectroscopy. *Industrial crops and products*, **20**(2): 205-218. <https://doi.org/10.1016/j.indcrop.2004.04.022>
- Daud, N. M. A. N., Jaafar, W. M. K. W., Ismail, N., Junin, R., Manan, M. A. and Idris, A. K. (2021, May). Utilizing Lignosulfonate from Coconut Husk as Sacrificial Agent to Reduce Surfactant Adsorption. In *IOP Conference Series: Earth and Environmental Science*, **765**(1): 012021. IOP Publishing. DOI 10.1088/1755-1315/765/1/012021
- Daoub R. M. A., Elmubarak A. H., Misran M., Hassan E. A. and Osman M. E. (2018). Characterization and Functional Properties of Some Natural Acacia Gums. *Journal of the Saudi Society of Agricultural Sciences*, **17**(3): 241–249. <https://doi.org/10.1016/j.jssas.2016.05.002>
- Ebringerová A. and Heinze T. (2000). Naturally Occurring Xylans Structures, Isolation Procedures and Properties. *Macromolecular Rapid Communications*, **21**(9): 542–556. [https://doi.org/10.1002/1521-3927\(20000601\)21:9%3C542::AID-MARC542%3E3.0.CO;2-7](https://doi.org/10.1002/1521-3927(20000601)21:9%3C542::AID-MARC542%3E3.0.CO;2-7)
- Elgibaly A. and Elkamel A. (1999). Optimal Hydrate Inhibition Policies with the Aid of Neural Networks. *Energy and fuels*, **13**(1): 105-113. <https://doi.org/10.1021/ef980129i>
- Farhadian A., Varfolomeev M. A., Kudbanov A. and Gallyamova S. R. (2019). A New Class of Promising Biodegradable Kinetic/Anti-Agglomerant Methane Hydrate Inhibitors based on Castor Oil. *Chemical Engineering Science*, **206**: 507–517. <https://doi.org/10.1016/j.ces.2019.05.055>
- Folger P. (2010). Gas Hydrates : Resource and hazard. Congressional Research Service. Available online at <https://fas.org/sgp/crs/misc/RS22990.pdf>. Retrieved on 4th November 2020.
- Gupta P. and Sangwai J. S. (2019). Formation and Dissociation Kinetics of Methane Hydrate in Aqueous Oilfield Polymer Solutions (Polyacrylamide, Xanthan Gum, and Guar Gum) and their Performance Evaluation as Low-Dosage Kinetic Hydrate Inhibitors (LDHI). *Energy and Fuels*, **33**(7): 6335–6349. <https://doi.org/10.1021/acs.energyfuels.9b01204>
- Igboanusi U.P. and Opara A.C. (2011). The Advancement from Thermodynamic Inhibitors to Kinetic Inhibitors and Anti-Agglomerants in Natural Gas Flow Assurance. *International Journal of Chemical and Environmental Engineering*, **2**: 2–5.
- Ishmuratov F. G., Rakhimova N. T., Ishmiyarov E. R., Voloshin A. I., Gusakov V. N., Tomilov Y. V., Nifant'yev N. E. and Dokichev V. A. (2018). New “Green” Polysaccharidal Inhibitor of Gas Hydrate Formation on the Basis of Carboxymethylcellulose Sodium Salt. *Russian Journal of Applied Chemistry*, **91**(4): 653–656. <https://doi.org/10.1134/S1070427218040183>
- Jokandan E. F., Naeiji P. and Varaminian F. (2016). The Synergism of the Binary and Ternary Solutions Of Polyethylene Glycol, Polyacrylamide and Hydroxyethyl Cellulose to Methane Hydrate Kinetic Inhibitor. *Journal of Natural Gas Science and Engineering*, **29**: 15–20. <https://doi.org/10.1016/j.jngse.2015.12.016>
- Kamal M. S., Hussein I. A., Sultan A. S. and Von Solms N. (2016). Application of

- Various Water Soluble Polymers in Gas Hydrate Inhibition. *Renewable and Sustainable Energy Reviews*, **60**: 206–225.
<https://doi.org/10.1016/j.rser.2016.01.092>
- Lemes, A. P., Soto-Oviedo, M. A., Waldman, W. R., Innocentini-Mei, L. H. and Durán, N. (2010). Effect of lignosulfonate on the thermal and morphological behavior of poly (3-hydroxybutyrate-co-3-hydroxyvalerate). *Journal of Polymers and the Environment*, **18**(3): 250-259.
- Makogon Y.F., Holditch S.A., Perry K.F. and Holste J.C. (2004). Gas Hydrate Deposits: Formation and Development. In *Offshore Technology Conference. OnePetro*.
<https://doi.org/10.4043/16677-MS>
- Mbuna J. J. and Mhinzi G. S. (2003). Evaluation of Gum Exudates from three Selected Plant Species from Tanzania for Food and Pharmaceutical Applications. *Journal of the Science of Food and Agriculture*, **83**(2): 142-146.
<https://doi.org/10.1002/jsfa.1279>
- Nita A. P., Azis M. M. and Suryo P. (2019). A Comparison of Sodium Lignosulfonate (SlS) Synthesis from Black Liquor Lignin and Commercial Lignin. *Materials Science Forum*, **94**(8): 206–211.
<https://doi.org/10.4028/www.scientific.net/MSF.948.206>
- Okereke N. U., Edet P. E., Baba Y. D., Izuwa N. C., Kanshio S. and Nwogu N. (2020). An Assessment of Hydrates Inhibition in Deepwater Production Systems using Low - Dosage Hydrate Inhibitor and Monoethylene Glycol. *Journal of Petroleum Exploration and Production Technology*, **10**(3): 1169–1182. <https://doi.org/10.1007/s13202-019-00812-4>
- Paez J.E. and Blok R. (2001). Problems in Hydrates: Mechanisms and Elimination Methods. In *SPE Production and Operations Symposium. OnePetro*.
<https://doi.org/10.2118/67322-MS>
- Paez J.E. and Blok R. (2001). Problems in Gas Hydrates: Practical Guidelines for Field Remediation. In *SPE Latin American and Caribbean Petroleum Engineering Conference. OnePetro*.
<https://doi.org/10.2118/69424-MS>
- Panamgama A.L. and Peramune P.S.K. (2018). Coconut Coir Pith Lignin: A Physicochemical and Thermal Characterization. *International Journal of Biological Macromolecules*, **113**: 1149–1157.
<https://doi.org/10.1016/j.ijbiomac.2018.03.012>
- Peng F., Ren J. L., Xu F., Bian J., Peng P. and Sun R. C. (2009). Comparative Study of Hemicelluloses obtained by Graded Ethanol Precipitation from Sugarcane Bagasse. *Journal of Agricultural and Food Chemistry*, **57**(14): 6305–6317.
<https://doi.org/10.1021/jf900986b>
- Perfeldt C. M., Chua P. C., Daraboina N., Friis D., Kristiansen E., Ramløv H., Woodley J. M., Kelland M. A. and Von Solms N. (2014). Inhibition of Gas Hydrate Nucleation and Growth: Efficacy of an Antifreeze Protein from the Longhorn Beetle *Rhagium Mordax*. *Energy and Fuels*, **28**(6): 3666–3672.
<https://doi.org/10.1021/ef500349>
- Perrin A., Musa O. M. and Steed J. W. (2013). The Chemistry of Low Dosage Clathrate Hydrate Inhibitors. *Chemical Society Reviews*, **42**(5): 1996–2015.
<https://doi.org/10.1039/c2cs35340>
- Plengnok U. and Jarukumjorn K. (2020). Preparation and Characterization of Nanocellulose from Sugarcane Bagasse. *Biointerface Research in Applied Chemistry*, **10**(3): 5675–5678.
<https://doi.org/10.33263/BRIAC103.675678>
- Qi G., Peng F., Xiong L., Lin X., Huang C., Li H., Chen X. and Chen X. (2017). Extraction and Characterization of Wax from Sugarcane Bagasse and the Enzymatic Hydrolysis of Dewaxed Sugarcane Bagasse. *Preparative Biochemistry and Biotechnology*, **47**(3): 276–281.
<https://doi.org/10.1080/10826068.2016.1224246>
- Tejado, A., Pena, C., Labidi, J., Echeverria, J. M. and Mondragon, I. (2007). Physico-chemical characterization of lignins from different sources for use in phenol–formaldehyde resin synthesis. *Bioresource*

- technology, **98**(8): 1655-1663.
<https://doi.org/10.1016/j.biortech.2006.05.042>
- Thungphotrakul, N., Dittanet, P., Loykulnunt, S., Tanpichai, S. and Parpainainar, P. (2019, June). Synthesis of sodium lignosulfonate from lignin extracted from oil palm empty fruit bunches by acid/alkaline treatment for reinforcement in natural rubber composites. In IOP Conference Series: Materials Science and Engineering, **526**(1), 012022). IOP Publishing, DOI 10.1088/1757-899X/526/1/012022
- Sa J. H., Kwak G. H., Lee B. R., Park D. H., Han K. and Lee K. H. (2013). Hydrophobic Amino Acids as a New Class of Kinetic Inhibitors for Gas Hydrate Formation. *Scientific Reports*, **3**: 1–7.
<https://doi.org/10.1038/srep02428>
- Sami N.A., Sangwai J. and Subramanian B. (2013). Gas Hydrate Applications and Problems in Oil And Gas Industry. *International Journal of Scientific and Engineering Research*. **4**: 1-5.
- Sanatgar S. M. and Peyvandi K. (2019). New Edible Additives as Green Inhibitors for Preventing Methane Hydrate Formation. *Journal of Environmental Chemical Engineering*, **7**(3): 103-172.
<https://doi.org/10.1016/j.jece.2019.103172>
- Setiati, R., Siregar, S., Marhaendrajana, T. and Wahyuningrum, D. (2018). Sustainable Innovation System Using Process of Bagasse Become Sodium Lignosulfonate Surfactant For Enhanced Oil Recovery. In E3S Web of Conferences, **43**: 01026). EDP Sciences.
<https://doi.org/10.1051/e3sconf/20184301026>
- Sun J. X., Sun X. F., Sun R. C. and Su Y. Q. (2004). Fractional Extraction and Structural Characterization of Sugarcane Bagasse Hemicelluloses. *Carbohydrate Polymers*, **56**(2): 195–204.
<https://doi.org/10.1016/j.carbpol.2004.02.002>
- Wan L., Zhang N. and Liang D. (2019). Inhibition Effects of Polysaccharides for Gas Hydrate Formation in Methane – Water System. *Journal of Molecular Liquids*, **29**(2): 111-435.
<https://doi.org/10.1016/j.molliq.2019.111435>
- Vázquez-Torres, H., Canché-Escamilla, G. and Cruz-Ramos, C. A. (1992). Coconut husk lignin. I. Extraction and characterization. *Journal of applied polymer science*, **45**(4): 633-644.
<https://doi.org/10.1002/app.1992.070450410>
- Xie Y., Guo X., Ma Z., Gong J., Wang H. and Lv Y. (2020). Efficient Extraction and Structural Characterization of Hemicellulose from Sugarcane Bagasse Pith. *Polymers*, **12**: 608.
<https://doi.org/10.3390/polym12030608>
- Xu, Z. P. and Braterman, P. S. (2003). High affinity of dodecylbenzene sulfonate for layered double hydroxide and resulting morphological changes. *Journal of Materials Chemistry*, **13**(2): 268-273.
<https://doi.org/10.1039/B207540G>
- Xu S., Fan S., Fang S., Lang X., Wang Y. and Chen J. (2016). Pectin as an Extraordinary Natural Kinetic Hydrate Inhibitor. *Scientific Reports*, **6**: 1–7.
<https://doi.org/10.1038/srep23220>
- Zarinabadi S., Samimi A., Branch S. and Branch M. (2011). Problems of Hydrate Formation in Oil and Gas Pipes Deals. *Australian Journal of Basic and Applied Science*, **5**(12): 741–745.
- Zhang, Y. T., Chen, F. L., Yu, S. J. and Wang, F. (2020). Biopromoters for gas hydrate formation: a mini review of current status. *Frontiers in chemistry*, **8**: 514.
<https://doi.org/10.3389/fchem.2020.00514>